Inorg. Chem. **2003**, *42*, 6859–6867

Hydrothermal Synthesis in the System $Ni(OH)_2$–$NiSO_4$: Nuclear and Magnetic Structures and Magnetic Properties of $Ni_3(OH)_2(SO_4)_2(H_2O)_2$

Serge Vilminot,*,† Mireille Richard-Plouet,† Gilles André,‡ Dariusz Swierczynski,† Françoise Bourée-Vigneron,‡ and Mohamedally Kurmoo†

Groupe des Matériaux Inorganiques, IPCMS, UMR 7504, 23 Rue du Loess, BP 43, 67034 Strasbourg Cedex 2, France, and Laboratoire Léon Brillouin, CEA-CNRS, CEA-Saclay, 91191 Gif-sur-Yvette Cedex, France

Received May 21, 2003

We present the synthesis, characterization by DT-TGA and IR, single crystal X-ray nuclear structure at 300 K, nuclear and magnetic structure from neutron powder diffraction on a deuterated sample at 1.4 K, and magnetic properties as a function of temperature and magnetic field of $Ni_3(OH)_2(SO_4)_2(H_2O)_2$. The structure is formed of chains, parallel to the *c*-axis, of edge-sharing $Ni(1)O_6$ octahedra, connected by the corners of $Ni(2)O_6$ octahedra to form corrugated sheets along the *bc*-plane. The sheets are connected to one another by the sulfate groups to form the 3D network. The magnetic properties measured by ac and dc magnetization, isothermal magnetization at 2 K, and heat capacity are characterized by a transition from a paramagnet ($C = 3.954$ emu K/mol and $\theta = -31$ K) to a canted antiferromagnet at $T_N = 29$ K with an estimated canting angle of 0.2–0.3°. Deduced from powder neutron diffraction data, the magnetic structure is modeled by alternate pairs of Ni(1) within a chain having their moments pointing along [010] and [0$\bar{1}$0], respectively. The moments of Ni(2) atoms are oppositely oriented with respect to their adjacent pairs. The resulting structure is that of a compensated arrangement of moments within one layer, comprising one ferromagnetic and three antiferromagnetic superexchange pathways between the nickel atoms.

Introduction

Hydroxy-sulfates of the d- and f-elements have been carefully studied by mineralogists,[1] where the principal interests were the identification of the crystal phases and the mechanism of their formation with respect to their geographic location. Such compounds are usually the result of sulfide degradation in the presence of water. Only the crystal structures of the most abundant forms have been characterized, and there are more phases that are not characterized due to the lack of single crystals in the natural sources of sufficient purity and quality. With the advances in hydrothermal synthesis, some of these missing links could be realized in the laboratory and on a shorter time scale. Furthermore, compounds prepared by hydrothermal method in the laboratory allow one to study the properties of pure samples, whereas samples from the mineral source are usually quite complex due to the presence of mixtures or traces of several cations and anions. In the case of transition metal hydroxy-sulfates, studies of their magnetic properties are sparse as a result of the low purity of samples from the mineral source. In the case of copper hydroxy-sulfates, hydrothermal synthesis gave two compounds that are isostructural with the corresponding minerals, antlerite $Cu_3(OH)_4SO_4$ and brochantite $Cu_4(OH)_6SO_4$.[2,3] No other phase was obtained under all the experimental conditions attempted. In a recent study of the structural and magnetic properties of synthetic antlerite,[4] we established the presence of edge-sharing copper octahedra forming chains. According to the value of the Cu−O−Cu bridge angle,[5−10] we anticipate that both ferro- and antiferromagnetic superexchange interactions

* Corresponding author. E-mail: vilminot@ipcms.u-strasbg.fr. Phone: +33-388 10 71 30. Fax: +33 388 10 72 47.
† Groupe des Matériaux Inorganiques, IPCMS.
‡ Laboratoire Léon Brillouin, CEA-CNRS.

(1) Eby, R. K.; Hawthorne, F. C. *Acta Crystallogr.* **1993**, *B49*, 28−56.
(2) Hawthorne, F. C.; Groat, L. A.; Eby, R. K. *Can. Mineral.* **1989**, *27*, 205−209.
(3) Helliwell, M.; Smith, J. V. *Acta Crystallogr.* **1997**, *C53*, 1369−1371.
(4) Vilminot, S.; Richard-Plouet, M.; André, G.; Swierczynski, D.; Guillot, M.; Bourée-Vigneron, F.; Drillon, M. *J. Solid State Chem.* **2003**, *170*, 255−264.
(5) Goodenough, J. B. *J. Phys. Chem. Solids* **1958**, *6*, 287−297.
(6) Kanamori, J. *J. Phys. Chem. Solids* **1959**, *10*, 87−98.
(7) Ginsberg, A. P. *Inorg. Chem. Acta, Rev.* **1971**, *5*, 45−68.

10.1021/ic0345469 CCC: $25.00
Published on Web 09/17/2003

are possible within one chain that we finally confirmed by analysis of the neutron diffraction data and modeling of the temperature dependence of the magnetic susceptibility.[4] Similar studies on transition metal(III) jarosites, $AB_3(SO_4)_2(OH)_6$ (where A = Na^+, K^+, Rb^+, Ag^+, H_3O^+, $^1/_2Pb^{2+}$ and B = Fe^{3+}, Cr^{3+}, V^{3+}), have also established a plethora of interesting magnetic properties.[11−13] The principal interest in the jarosites is the presence of a kagomé lattice and the problems associated with frustration of a triangular magnetic lattice. Using another approach, existing mineral lattices can be functionalized with organic units; an example of such a system is the modification of the layered namuwite structure,[14−16] $(Zn,Cu)_4SO_4(OH)_6\cdot 4H_2O$, (a) by exchanging the diamagnetic cations (M^{II}) for paramagnetic ones and (b) by introducing a chemical connection between the layers via an organic pillar (e.g., a diamine) to produce unusual porous magnets, $M^{II}_4(OH)_6(SO_4)(pillar)_{0.5}\cdot xH_2O$.[17] These results have stimulated the present study using the same techniques for other divalent transition metal $M(OH)_2-MSO_4$ systems. In the case of M = Ni, four compounds have been obtained by hydrothermal synthesis under various conditions: temperatures ranging from 120 to 240 °C and different concentrations of reactants as the two main parameters. In the literature,[18] only one mineral of high nickel content is known, paraotwayite, corresponding to $Ni_{0.99}Mg_{0.01}(OH)_{1.43}(SO_4)_{0.17}(CO_3)_{0.12}\cdot 0.37H_2O$. This nickel basic sulfate has also been obtained by forced hydrolysis at 100 °C from a solution containing nickel nitrate, nickel sulfate, and sodium acetate.[19] Needlelike particles have been obtained, but their chemical compositions have not been determined. The present study in the system $Ni(OH)_2-NiSO_4$ under hydrothermal conditions resulted in the formation of the related phase $Ni_5(OH)_8SO_4\cdot 3H_2O$, that appears to be isomorphous with paraotwayite, and of three other phases: $Ni_5(OH)_6(SO_4)_2\cdot 3H_2O$, $Ni_5(OH)_6(SO_4)_2$, and $Ni_3(OH)_2(SO_4)_2(H_2O)_2$. Single crystals have been obtained only for the latter, and this paper focuses on the determination of the nuclear and magnetic structures and the magnetic properties of $Ni_3(OH)_2(SO_4)_2(H_2O)_2$.

Experimental Section

Synthesis. The title compound was prepared by hydrothermal treatment of an aqueous suspension of nickel sulfate heptahydrate, $NiSO_4\cdot 7H_2O$, and NaOH in various Ni/Na molar ratios at temperatures higher than 210 °C. The stoichiometry of the title compound is $2NiSO_4\cdot 1Ni(OH)_2$; interestingly, it is obtained for all explored ratios between $7NiSO_4/1Ni(OH)_2$ and $1NiSO_4/1Ni(OH)_2$. Single crystals as strongly agglomerated green rectangular platelets were obtained with higher dilutions, typically with molar ratios Ni/Na/H_2O = 1:0.25:250. However, it is difficult to obtain a pure phase, and in most cases, the presence of one of the other hydroxy-sulfates is evidenced as a very minor phase by X-ray diffraction. The reactions were performed under autogenous pressure in autoclaves of 125 cm^3, with a filling ratio around $^1/_3$. The precursor suspension is stirred for 1 h before sealing in the reactor that was heated at 215, 230, or 240 °C for 1−4 days. After this period, the green crystals were retrieved by filtration and washed with water and acetone.

Table 1. Summary of X-ray Data Collection on a Single Crystal and Structure Refinement of $Ni_3(OH)_2(SO_4)_2(H_2O)_2$

a (Å)	7.1485(3)	μ (mm^{-1})	6.89
b (Å)	9.6844(4)	total reflns	3722
c (Å)	12.6643(3)	unique reflns	1323
V ($Å^3$)	876.74(6)	unique $\lvert F_o\rvert > 4\sigma(F_o)$	1252
Z	4	R_{int}	0.0254
space group	*Pbcm* (No. 57)	$R(F)$ (all data)[a]	0.0335
$F(000)$	848	$R_w(F_o^2)$ (all data)	0.0847
D_c ($g\cdot cm^{-3}$)	3.319	GOF	1.12

[a] $R(F) = \sum||F_o| - |F_c||/\sum|F_o|$. [b] $R_w = \{\sum[w(F_o^2 - F_c^2)^2]/\sum[w(F_o^2)^2]\}^{1/2}$, $w = 1/[\sigma^2(F_o^2) + (0.0492P)^2 + 0.96P]$ with $P = (\max(F_o^2, 0) + 2F_c^2)/3$.

Samples for neutron diffraction measurements were synthesized in the same conditions starting from $NiSO_4\cdot 7H_2O$, NaOH, and D_2O. The synthesis always yield a two phase mixture, $Ni_5(OH)_6(SO_4)_2$ being the secondary phase evidenced from X-ray diffraction powder data. The use of D_2O is to reduce the effect of the high neutron incoherent diffusion factor of hydrogen giving rise to an increase of the background and a poor signal-to-background ratio that can deteriorate further analysis. Many attempts were performed to avoid the secondary phase formation, but we did not succeed. The samples chosen for the experiments contain the least amount of the second phase.

General Characterizations. Thermal analysis was performed with a DT-TGA92 SETARAM apparatus, at a 3.5 °C/min heating rate, under air. Infrared spectra were recorded on an ATI Mattson spectrometer using the KBr pellet technique. Powder X-ray diffraction patterns were recorded using a D5000 Siemens diffractometer (Cu $K\alpha_1$, 1.5406 Å).

Xray Crystallography and Nuclear Structure Solution. For single crystal X-ray data collection at room temperature, a single set of 180 frames, 20 s/frame, φ scan of 1 deg/frame (each frame measured twice), crystal detector distance = 30 mm, $\theta = 0°$, $\kappa = 0°$ was collected on a Nonius Kappa CCD diffractometer at the Service Commun de Rayons X, Université Louis Pasteur, Strasbourg. The structure was solved by means of a three-dimensional Patterson function allowing us to find the positions of Ni ions. Subsequent parameter refinement cycles and three-dimensional difference Fourier maps using SHELX93 yield the positions of all atoms.[20] The final refinement includes anisotropic displacement parameters and a secondary extinction correction. The atomic coordinates of hydrogen atoms were not refined. Additional experimental details are given in Table 1 and in Supporting Information (Table S1). Table 2 gives the interatomic distances and angles from X-ray refinement. The oxygen atoms of the sulfate group, of the hydroxyl groups, and of the water molecule have been

(8) Hay, P. J.; Thibeault, J. C.; Hoffmann, R. *J. Am. Chem. Soc.* **1975**, *97*, 4884−4898.
(9) Crawford, V. H.; Richardson, H. W.; Wasson, J. R.; Hodgson, D. J.; Hatfield, W. E. *Inorg. Chem.* **1976**, *15*, 2107−2110.
(10) Weihe, H.; Güdel, H. U. *J. Am. Chem. Soc.* **1998**, *120*, 2870−2879.
(11) Wills, A. S. *Phys. Rev.* **2001**, *B63*, 064430.
(12) Wills, A. S.; Harrison, A.; Ritter, C.; Smith, R. I. *Phys. Rev.* **2000**, *B61*, 6156−6169.
(13) Papoutsakis, D.; Grohol, D.; Nocera, D. G. *J. Am. Chem. Soc.* **2002**, *124*, 2647−2656.
(14) Bevins, R. E.; Turgoose, S.; Williams, P. A. *Mineral. Mag.* **1982**, *46*, 51.
(15) Groat, L. A. *Am. Mineral.* **1996**, *81*, 238−243.
(16) Rujiwatra, A.; Kepert, C. J.; Rosseinsky, M. J. *Chem. Commun.* **1999**, 2307−2308.
(17) Rujiwatra, A.; Kepert, C. J.; Claridge, J. B.; Rosseinsky, M. J.; Kumagai, H.; Kurmoo, M. *J. Am. Chem. Soc.* **2001**, *123*, 10584−10594.
(18) Nickel, E. H.; Graham, J. *Can. Mineral.* **1987**, *25*, 409−411.
(19) Ocaña, M. *J. Colloid Interface Sci.* **2000**, *228*, 259−262.
(20) Sheldrick, G. M. *SHELXL-93, Program for the Refinement of Crystal Structures*; University of Göttingen: Göttingen, Germany, 1993.

Table 2. Interatomic Distances (Å) and Angles (deg) from X-ray Structure Determination (Upper Part) and Involving D Atoms from Neutron Powder Diffraction Data at 300 K (Lower Part)

S1−O3	1.455(2) ×2	O3−S1−O3	107.56(15)	O2−S1−O2	108.85(15)
S1−O2	1.493(2) ×2	O3−S1−O2	110.18(10) ×2	⟨O−S1−O⟩	109.5
⟨S−O⟩	1.474	O3−S1−O2	110.04(10) ×2		
S2−O4	1.458(2)	O4−S2−O1	110.66(15)	⟨O−S2−O⟩	109.5
S2−O1	1.475(3)	O4−S2−O5	108.44(10) ×2		
S2−O5	1.476(3) ×2	O1−S2−O5	110.17(10) ×2		
⟨S−O⟩	1.472	O5−S2−O5	108.91(16)		
Ni1−O5	2.034(2)	O5−Ni1−OH1	94.40(9)	OH1−Ni1−O2	101.97(7)
Ni1−OH1	2.039(2)	O5−Ni1−OW	167.58(8)	OW−Ni1−OH2	102.73(9)
Ni1−OW	2.046(2)	O5−Ni1−OH2	88.86(8)	OW−Ni1−O2	84.27(8)
Ni1−OH2	2.077(2)	O5−Ni1−O2	89.30(8)	OW−Ni1−O2	86.12(8)
Ni1−O2	2.152(2)	O5−Ni1−O2	82.10(7)	OH2−Ni1−O2	100.54(7)
Ni1−O2	2.173(2)	OH1−Ni1−OW	91.86(9)	OH2−Ni1−O2	170.70(8)
⟨Ni1−O⟩	2.087	OH1−Ni1−OH2	80.83(7)	O2−Ni1−O2	77.25(7)
		OH1−Ni1−O2	176.09(8)		
Ni2−O3	2.009(2) ×2	O3−Ni2−O3	165.73(11)	OH1−Ni2−O4	95.09(10)
Ni2−OH1	2.031(2)	O3−Ni2−OH1	90.98(5) ×2	OH1−Ni2−O1	173.52(10)
Ni2−OH2	2.045(2)	O3−Ni2−OH2	97.02(5) ×2	OH2−Ni2−O4	172.53(10)
Ni2−O4	2.093(2)	O3−Ni2−O4	82.87(5) ×2	OH2−Ni2−O1	94.10(10)
Ni2−O1	2.108(3)	O3−Ni2−O1	88.23(5) ×2	O4−Ni2−O1	78.43(10)
⟨Ni2−O⟩	2.049	OH1−Ni2−OH2	92.38(9)		
Ni1···Ni1	3.067(2)	Ni1−OH1−Ni1	97.6(1)	Ni1−O2−Ni1	102.75(7)
Ni1···Ni1	3.380(2)	Ni1−OH2−Ni1	95.3(1)	Ni1−OH1−Ni2	124.89(7)
				Ni1−OH2−Ni2	118.93(8)
OD1−D1	0.999(8)	D1···O1	1.935(8)	OD1−D1···O1	163(4)
OD2−D2	0.992(8)	D2···O5	2.299(6) ×2	OD2−D2···O5	146(2)
OW−DW1	0.849(5)	DW1···O3	2.195(6)	OW−DW1···O3	158(2)
OW−DW2	0.914(9)	DW2···O5	2.010(8)	OW−DW2···O5	156(3)

Table 3. Summary of the Crystallographic Data and Refinement Characteristics at 300 and 1.4 K from Neutron Powder Data for Deuterated Compound

	300 K	1.4 K		300 K	1.4 K
system	orthorhombic		no. params	54	48
space group	*Pbcm* (No. 57)		R_p (%)	6.52	9.05
a (Å)	7.14991(7)	7.1437(5)	R_{wp} (%)	6.26	9.39
b (Å)	9.6832(1)	9.6468(6)	R_{exp} (%)	5.40	1.79
c (Å)	12.6676(1)	12.6320(9)	RB (%)	2.16	2.19
wavelength (Å)	1.2252	2.4266	RF (%)	1.31	1.95
2θ range, step	6−125.7°, 0.05°	9−88.9°, 0.1°	GOF (%)	1.35	
reflns used/total	1133/4103	455/626	$R_{magnetic}$ (%)		7.98

labeled as O, OH, and OW, respectively. For H(D for neutron data) atoms, H1(D1) and H2(D2) correspond to OH1(OD1) and OH2-(OD2) groups, respectively, whereas HW (DW) refers to the H(D) atoms of the water molecule. The structure data have been deposited at Fachinformationszentrum (FIZ) Karlsruhe and have been given CSD-number 413179.

Neutron Crystallography and Magnetic Structure Solution. The neutron diffraction experiments were performed at the Laboratoire Léon Brillouin (CEA Saclay) using the G4.1 and 3T2 diffractometers. The multidetector (800 cells) G4.1 powder diffractometer ($\lambda = 2.4266$ Å) was used for the resolution of the magnetic structure and the study of the evolution of the low temperature patterns. Therefore, 13 diffraction patterns were recorded in the 2θ range 9−88.9°, at different temperatures between 1.4 and 35.6 K. The powder sample was set in a cylindrical vanadium can and held in a liquid helium cryostat. The room temperature structure refinement was performed from data collected on the high resolution 3T2 powder diffractometer ($\lambda = 1.2251$ Å). Nuclear and magnetic structures were refined using the Rietveld-type FULLPROF[21] program. The nuclear scattering lengths ($b_{Ni} = 1.0300 \times 10^{-12}$ cm, $b_S = 0.2847 \times 10^{-12}$ cm, $b_O = 0.5803 \times 10^{-12}$ cm, $b_D = 0.6671 \times 10^{-12}$ cm, and $b_H = -0.3739 \times 10^{-12}$ cm) and nickel magnetic form factors were those included in this program. Table 3 summarizes data collection conditions; values concerning hydrogen bonding from powder neutron data are given in Table 2, and other data are appended in the Supporting Information (Tables S1 and S2).

Magnetic Properties. Magnetization measurements were performed in the range 2−300 K and at an applied field of 5 and 100 Oe by means of a Quantum Design MPMS-XL SQUID magnetometer. Alternating current measurements were performed with the same apparatus in zero dc field and an alternating field of 1 Oe oscillating at 17 Hz. Isothermal magnetization was measured at 2 K in field spanning ±50 kOe. The sample was first cooled in zero field. The sample was prepared by selecting several large crystals under a microscope and then washing them with ethanol in an ultrasonic bath to remove most of the fine powder of the second phase. The large crystals were then separated by decantation. This procedure reduced the content of the other phases considerably as they exist as fine particles that remain in the decanted suspension. The sample (14.22 mg) was placed in a gelatine capsule for the measurements. We did not observe any torque of the sample up to 50 kOe. Specific heat measurements between 1.7 and 38 K were carried out in zero-field with home-built equipment using a quasi-adiabatic method.

Results

Hydrothermal synthesis allows new compounds in the binary system $Ni(OH)_2-NiSO_4$ to be obtained. Since Ni_3-

(21) Rodriguez-Carvajal, J. *FULLPROF: Rietveld, profile matching and integrated intensity refinement of X-ray and/or neutron data*, 3.5d version; Léon-Brillouin Laboratory: CEA Saclay, France, 1998.

$(OH)_2(SO_4)_2(H_2O)_2$ was obtained as single crystals, we focus our study on this phase. However, it has to be noted that the preparation of a pure monophase sample appears very difficult.

Thermal Behavior. The thermogravimetry trace (Supporting Information, Figure S1) reveals three weight loss steps between 390 and 885 °C. The first one between 390 and 495 °C corresponds to the loss of two water molecules (obsd 7.54 wt %, calcd 8.09 wt %) according to

$$Ni_3(OH)_2(SO_4)_2(H_2O)_2 \rightarrow Ni_3(OH)_2(SO_4)_2 + 2H_2O$$

It is associated with an endothermal effect centered at 465 °C. Assuming the compound contains water molecules (see infrared results), the high temperature of their departure excludes the presence of hydration molecules. Therefore, the water molecules are expected to be strongly coordinated to the nickel ion. X-ray diffraction of a sample heated to 495 °C reveals the formation of an amorphous phase, probably in relation to the water loss yielding a collapse of the structure. The second weight loss between 510 and 610 °C, with a related endothermal effect centering at 589 °C, corresponds to the loss of one water molecule, probably related to the departure of two OH groups (obsd 3.77 wt %, calcd 4.04 wt %) according to

$$Ni_3(OH)_2(SO_4)_2 \rightarrow NiO + 2NiSO_4 + H_2O$$

X-ray diffraction of a sample heated to 610 °C reveals the presence of only NiO, suggesting that $NiSO_4$ is possibly amorphous.

Finally, at high temperature, between 655 and 885 °C, sulfate groups decompose as SO_3 (obsd 36.49 wt %, calcd 36.84 wt %) yielding only NiO, confirmed by XRPD, as final residue (obsd 50.80 wt %, calcd 51.14 wt %). The center of the associated endothermal effect is at 820 °C.

Infrared Spectroscopy. The infrared spectrum (Supporting Information, Figure S2) reveals the presence of bands related to the following: O−H valence stretching modes in the region 3540−3440 cm^{-1}, H_2O bending mode at 1619 cm^{-1}, ν_3 and ν_4 internal modes of the SO_4^{2-} ions around 1100 and 600 cm^{-1}, and O−H libration modes around 800 cm^{-1}.

In the deuterated sample, the O−H valence stretching bands are shifted to 2636 and 2543 cm^{-1}, values already found in the case of antlerite, $Cu_3(OD)_4SO_4$.[4] Water is clearly evidenced from the sharp band at 1619 cm^{-1} that is shifted to 738 cm^{-1} in the deuterated sample. ν_3 and ν_4 vibrations of the SO_4 tetrahedra appear as well-resolved bands. Clearly, three bands (1202, 1159, and 1109 cm^{-1}) whose positions do not change in the deuterated compound are evidenced in the ν_3 region as well as three bands (648, 627, and 600 cm^{-1}) in the ν_4 region. Two other bands appear at 1035 and 995 cm^{-1}, corresponding to the totally symmetric ν_1 stretching mode of the sulfate groups.

Structure Description. The asymmetric unit consists of two symmetry equivalent Ni(1) and one Ni(2), two different sulfur atoms, two hydroxide oxygen atoms, one water molecule, and the oxygen atoms of the sulfate groups. The

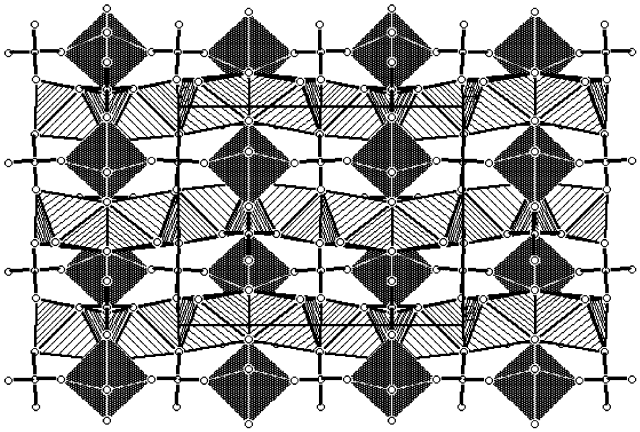

Figure 1. Projection of the structure of $Ni_3(OH)_2(SO_4)_2(H_2O)_2$ on the *bc* plane. Striped and gray polyhedra correspond to $Ni(1)O_6$ and $Ni(2)O_6$ octahedra, respectively, and sulfate is represented by ball-and-stick.

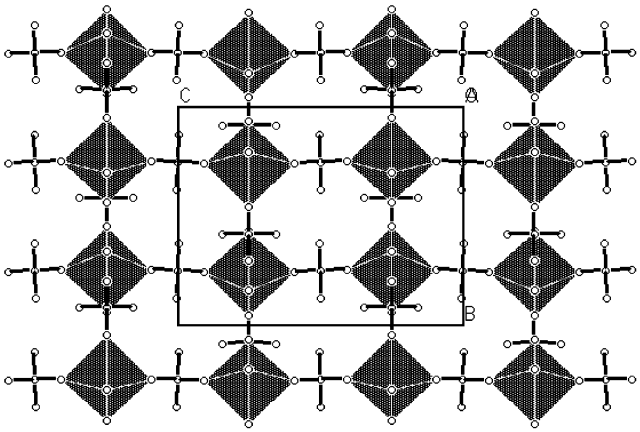

Figure 2. Projection on the *bc* plane showing the connections between Ni(2) octahedra and sulfate tetrahedra.

structure of $Ni_3(OH)_2(SO_4)_2(H_2O)_2$ can be broken down as follows (Figure 1). It consists of 1D chains of edge-sharing Ni(1) running along the *c*-axis. The oxygen atoms forming the bridges are of two types; they alternate in pairs, one pair from the hydroxides and the other from sulfates. The water molecules complete the octahedral coordination of Ni(1). Adjacent chains are connected into a corrugated layer via the *cis*-oxygen atoms (μ_3-OH) of the octahedra of Ni(2) and those of the sulfate groups (Figures 2 and 3). One can distinguish (Figure 2) Ni(2) octahedra, isolated from each other and connected by sulfate tetrahedra, either S1 along the *c*-axis direction or S2 along the *b*-axis direction. The 3D structure is generated by the connections of the layers via the sulfate groups. The Ni(1)−O distances in the chain have an average value of 2.058 Å for Ni−OH and Ni(1)−O(sulfate) values range from 2.034 to 2.173 Å. The corresponding Ni(2)−O values are 2.38 Å and from 2.009 to 2.108 Å. The corresponding Ni(2)−OH is 2.08 and 1.995 Å, and Ni(2)−O(sulfate) values range from 2.043 to 2.172 Å. The important angles, with respect to the observed magnetic properties (see later), have values for Ni(1)−OH−Ni(1) of 95.3° and 97.6°, for Ni(1)−$O_{sulfate}$−Ni(1) of 102.75°, and for Ni(1)−OH−Ni(2) of 124.9° and 118.9°. The nickel octahedra are distorted with angles involving opposite oxygen atoms in *trans*-positions close to 180° and those involving

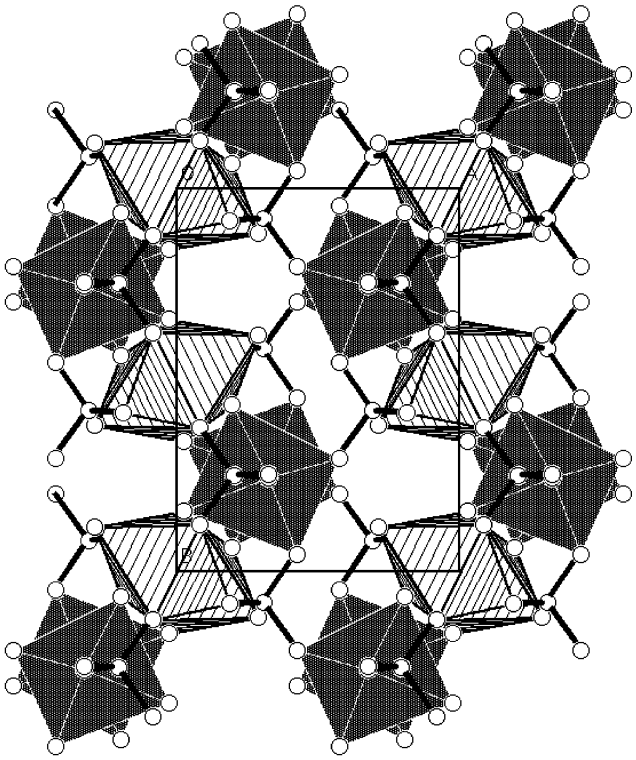

Figure 3. Projection on the *ab* plane showing the links between Ni(1) (striped) and Ni(2) (gray) octahedra building corrugated sheets.

cis-positions deviating up to 14% from 90°. The Ni−O bond lengths deviate by only 5% from the mean distance.

Two crystallographically independent sulfate groups are present in the structure. They both adopt a nearly regular tetrahedral geometry, and the S−O bond lengths have values expected for orthosulfates, ⟨S−O⟩ = 1.474 and 1.472 Å for S1 and S2, respectively. Both sulfate groups act as μ_4-bridges to generate the 3D architecture.

The O−H distances range from 0.66 to 0.92 Å, values usually observed for this kind of bond from X-ray diffraction data. All oxygen atoms but O2 (μ_3-oxo) are μ_2-oxo type whereas all oxygen atoms from OH groups are μ_3-oxo type.

Structure refinement from neutron powder data (Supporting Information, Figure S3) is in good agreement with the general features obtained from single crystal X-ray measurement, even if the refinement of the positions of the sulfur atom S2 yields a more distorted sulfate geometry, with S−O bond distances between 1.417(12) and 1.532(7) Å. The refinement also confirms that deuteration has been achieved at a high level with a D/(D + H) ratio of 0.87. The D atoms are involved in weak deuterium bonds, the shortest D···O distance being 1.935 Å (Table 2). Whereas D1, DW1, and DW2 define monofurcated deuterium bonds, D2 is shared between two oxygen atoms yielding a decrease of the O−D···O angle from around 160° to 146°. The observed and calculated neutron powder diffraction patterns are given in Supporting Information (Figure S3). They include the contribution of the impurity phase, as already mentioned, which is treated in the pattern-matching mode.

Magnetic Characterization. Susceptibility Measurements. In the paramagnetic region, the magnetic susceptibility follows the Curie−Weiss law $\chi = C/(T - \theta) = 3.954/(T + 31.23)$ emu·mol^{-1} calculated from the fit of the $1/\chi$ experimental data in the temperature range 130−300 K (Figure 4). $C = Ng^2\mu_B^2 s(s + 1)/3k$ is the Curie constant assuming a spin only value of $s = 1$ for nickel(II). The negative θ value and the decrease of the χT product suggest that the dominant exchange interaction is antiferromagnetic. From the Curie constant, we can deduce a g-value of 2.29 consistent with those observed for divalent nickel. Below around 100 K, the inverse susceptibility deviates from the Curie−Weiss behavior. A transition takes place at around 30 K that is characterized by a strong increase of the χ value that reaches a plateau at low temperature (Figure 4). The temperature dependence of the dc susceptibility in 5 Oe and of the ac susceptibilities is shown in Figure 5. Spontaneous magnetization is observed as a sharp transition at 29.6 K defining the long-range magnetic ordering. From the isothermal magnetization at 2 K, this transition is consistent with an antiferromagnetic long range ordering associated with a small canting of the sublattices. The ac susceptibilities are very sensitive to small amounts of the other phases that appear as a broad hump in addition to the sharp peaks at the

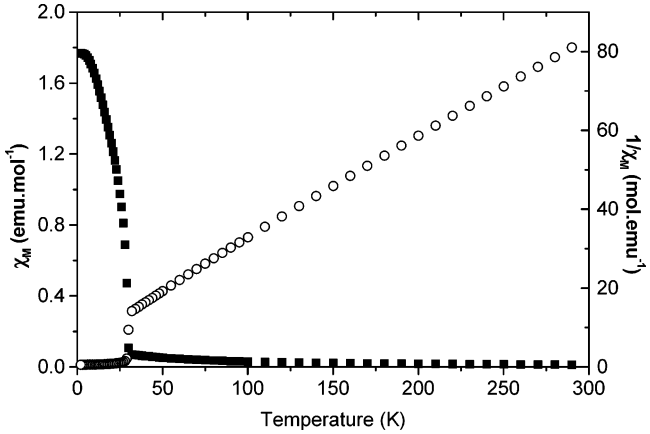

Figure 4. Magnetic susceptibility (■) and inverse magnetic susceptibility (○) versus temperature for $Ni_3(OH)_2(SO_4)_2(H_2O)_2$. (Magnetic susceptibility measured in an applied field of 100 Oe.)

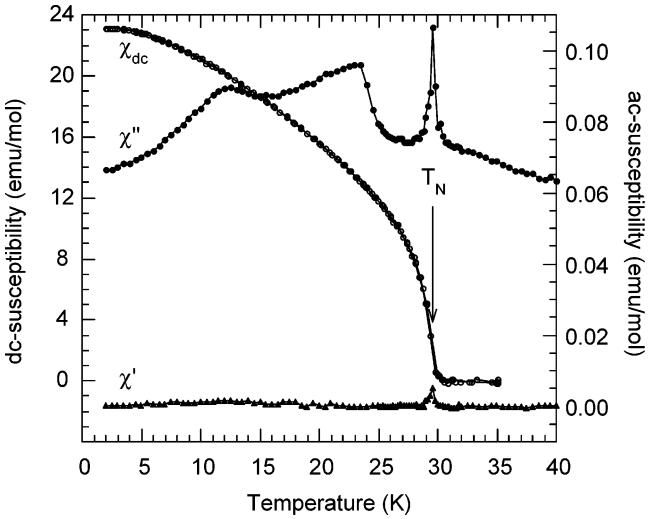

Figure 5. Temperature dependence of the ac magnetic susceptibilities measured in a 1 Oe field oscillating at 17 Hz and dc magnetic susceptibility measured on cooling in a field of 5 Oe.

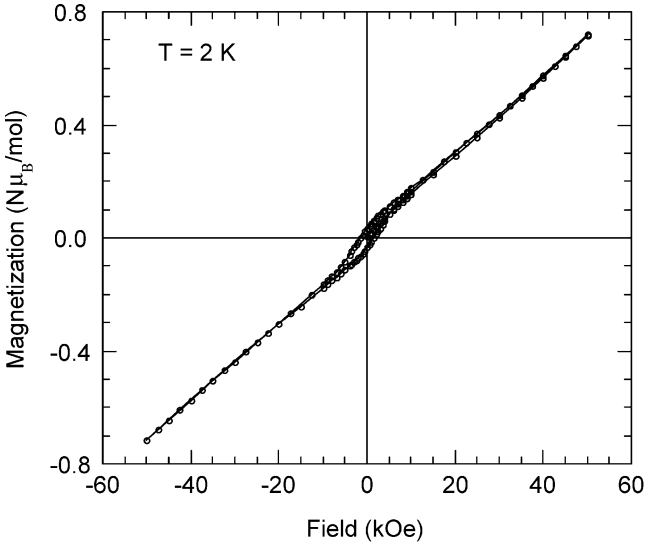

Figure 6. Isothermal magnetization versus applied field at 2 K for $Ni_3(OH)_2(SO_4)_2(H_2O)_2$.

Néel transition (T_N). The dc susceptibility in contrast does not exhibit any anomaly, suggesting that the impurities are present in very small quantities. The sharpness of the ac susceptibility is an indication of a very small canting angle. From the value of the magnetization measured at 2 K upon field-cooling in 5 Oe, we estimate a canting angle of 0.2° assuming a two sublattice antiferromagnet. The evolution of the magnetization with applied field at 2 K reveals the presence of a very narrow hysteresis loop (Figure 6) superimposed on a linear field dependent magnetization. These observations and the low value of the magnetization of only 0.7 μ_B in 50 kOe compared to a theoretical 6.0 μ_B, if all the moments were fully aligned with the field, are consistent with those of canted antiferromagnets. The estimation of the canting angle from the remanence magnetization value, according to $\alpha = \arcsin(M_{rem}/M_{sat})$ where M_{rem} is the remanent magnetization at 2 K and M_{sat} the expected saturation magnetization if all the moments are aligned ferromagnetically, is 0.3°, in fair agreement with that already estimated. The coercive field is 1.4 kOe at 2 K.

Specific Heat. Measurement at low temperature clearly confirms the presence of the 3D long ranged magnetic transition previously evidenced from susceptibility data with the occurrence of a λ-type anomaly with a maximum at around 29 K (Figure 7).

Magnetic Structure. The magnetic structure has been studied from neutron powder diffraction data collected at 13 temperatures between 1.4 and 36 K. Above 29 K, no extra Bragg peaks or enhancement of the nuclear Bragg peaks are observed. Below this temperature, some new lines with significant intensities appear on the corresponding diffractograms with decreasing temperature. These main lines can be indexed as (001), (101), (003), (201), and (005) using the nuclear cell parameters.

The possible influence of the impurity inside the sample, even at a very low proportion, has to be considered. The magnetic susceptibility of this phase, $Ni_5(OH)_6(SO_4)_2$,[22] follows a Curie−Weiss law in the 100−300 K range with a negative θ in relation with antiferromagnetic interactions. A transition toward a long-range antiferromagnetic ordered state takes place at 23 K, also confirmed by ac susceptibility measurements with a peak only in the real part. It is therefore expected that an AF structure will give rise to additional magnetic Bragg peaks. However, we could not assign any of the observed magnetic peaks to this impurity phase. First, all the observed magnetic lines were indexed in the crystallographic unit cell of the present compound, $Ni_3(OH)_2(SO_4)_2(H_2O)_2$. Second, we verify carefully the intensities and positions of all the magnetic peaks in the temperature range 23 and 29 K and compare them to those observed below 23 K. No other extra peaks are evidenced below 23 K that may be assigned to the impurity. It can therefore be inferred that the magnetic lines are only related to $Ni_3(OH)_2(SO_4)_2(H_2O)_2$.

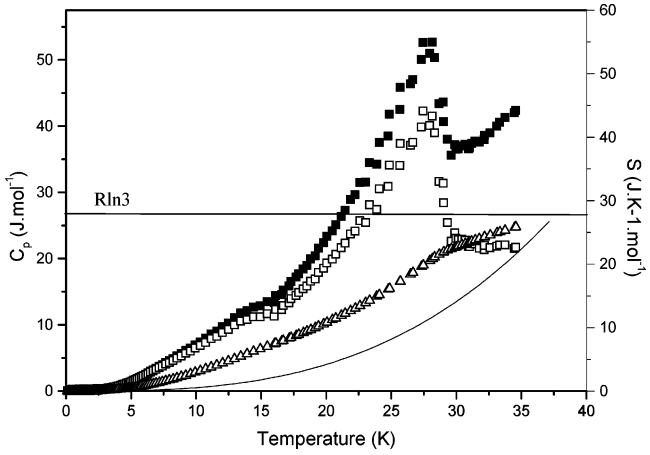

Figure 7. Specific heat evolution versus temperature: ■, experimental; □, magnetic contribution; —, lattice contribution; △, entropy.

Before proceeding to the determination of the magnetic structure, a refinement considering only the nuclear contributions of the two phases has been performed for the neutron powder data recorded at 1.4 K. We followed by determining the associated magnetic structure with the help of Bertaut's representation analysis method,[23] applied to the *Pbcm* space group, $k = (0\ 0\ 0)$ propagation vector and (8e) [Ni1] and (4d) [Ni2] Wyckoff positions. Eight one-dimensional irreducible representations (IRs) are determined,[24a] Γ_1 to Γ_8, which are associated to basis vectors (magnetic structures) for Ni1 and Ni2.[24b] Each Γ_i ($i = 1-8$) is involved in Ni1 and Ni2 "magnetic arrangements", according to

Ni1 (8e)

$$3\Gamma_1 + 3\Gamma_2 + 3\Gamma_3 + 3\Gamma_4 + 3\Gamma_5 + 3\Gamma_6 + 3\Gamma_7 + 3\Gamma_8$$

and

Ni2 (4d) $\quad \Gamma_1 + 2\Gamma_2 + \Gamma_3 + 2\Gamma_4 + 2\Gamma_5 + \Gamma_6 + 2\Gamma_7 + \Gamma_8$

(22) Swierczynski, D.; Vilminot, S. Unpublished results.
(23) Bertaut, E. F. *Acta Crystallogr.* **1968**, *A24*, 217.
(24) Hovestreydt, E.; Aroyo, I.; Sattler, S.; Wondratschek, H. KAREP—a program for calculating irreducible space group representations. *J. Appl. Crystallogr.* **1992**, *25*, 544. (b) Rodriguez-Carvajal, J. *BASIREPS—a program for calculating nonnormalized basis functions of the irreducible representations of the little group Gk for atom properties in a crystal*, Laboratoire Léon Brillouin: CEA-Saclay, France.

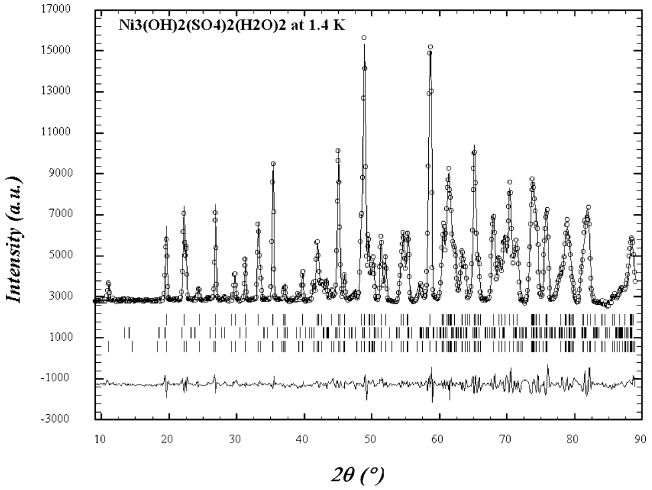

Figure 8. Observed (○) and calculated (—) profiles of the powder neutron pattern of $Ni_3(OD)_2(SO_4)_2(D_2O)_2$ obtained on the G4.1 diffractometer at 1.4 K with position of the Bragg reflections (short vertical lines, nuclear $Ni_3(OD)_2(SO_4)_2(D_2O)_2$, nuclear impurity, magnetic $Ni_3(OD)_2(SO_4)_2(D_2O)_2$) and difference between observed and calculated profiles.

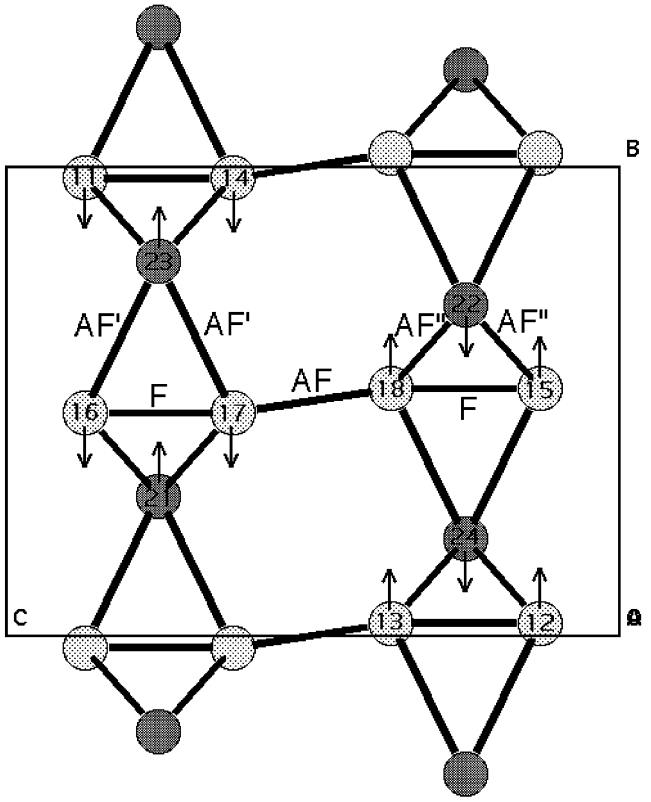

Figure 9. Projection of the structure on the bc plane showing the orientations of the magnetic moments within one layer (Ni(1) in light gray and Ni(2) in dark gray); the four types of superexchange pathways between the nickel atoms are indicated.

If solutions involving basis vectors associated to distinct Γ_i are not forbidden, one must first check for basis vectors within one Γ_i. In the present case, Γ_2 leads to the best magnetic reliability factor $R_M = 8.0\%$ (Figure 8), with magnetic moments along *b* (Figure 9) with values 2.00(4) and 1.67(6) μ_B for Ni1 and Ni2, respectively. The symmetry relations between Ni1*i* and Ni2*i* positions are given in Supporting Information (Table S2) as well as in parentheses in the following paragraph.

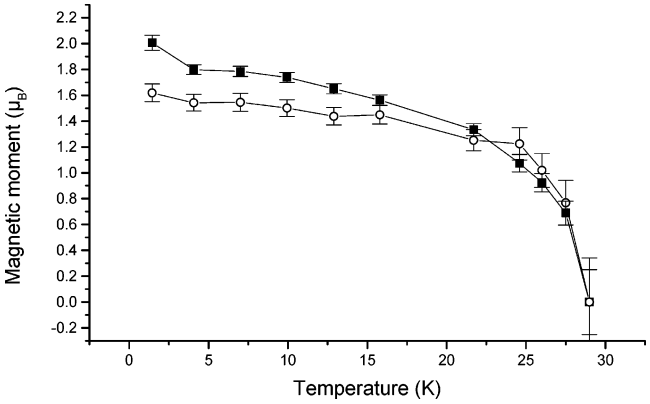

Figure 10. Thermal evolution of the Ni(1) (■) and Ni(2) (○) magnetic moments.

Let us note, however, that Γ_2 is associated to the subsequent magnetic arrangement

	M//**a**	M//**b**	M//**c**
Ni11− ··· −Ni18	+ − − + + − − +	+ − − + − + + −	+ − + − − + − +
Ni21− ··· − Ni24	+ − − +	+ − + −	

where the sequence + − − + + − − + for instance holds for the component of the magnetic moments of Ni11 to Ni18 atoms, as defined here, along the *a* crystallographic axis. (The symmetry relations between Ni11 to Ni18 are as follows: $x, y, z; -x, -y, -z; -x, -y, {}^1/_2 + z; x, y, {}^1/_2 - z; x, {}^1/_2 - y, -z; -x, {}^1/_2 + y, z; -x, {}^1/_2 + y, {}^1/_2 - z; x, {}^1/_2 - y, {}^1/_2 + z$. For Ni21 to Ni24, they are the following: $x, y, {}^1/_4; -x, -y, {}^3/_4; -x, {}^1/_2 + y, {}^1/_4; x, {}^1/_2 - y, {}^3/_4$.) Within Γ_2, no magnetic moment is allowed along *c* for Ni2 atoms.

As previously mentioned, all the magnetic lines have been indexed in the nuclear crystallographic unit cell, but all are associated to *(h*0*l)* which are forbidden within the *Pbcm* space group, namely *(h*0*l)* with *l* odd. This selection rule implies that magnetic moments of either Ni1 or Ni2 atoms, with the same *x* coordinate and *z* coordinate separated by $^1/_2$, are opposite to each other. In addition, we note that the above selection rule [*(h*0*l)* with *l* odd] only holds for Γ_2, *b* sequences.

This magnetic structure (Γ_2, magnetic moments along *b*) is observed for any *T* below T_N, and refinements of the data collected at low temperatures (1.4 K = *T* = 29 K) yield the thermal variations of Ni1 and Ni2 magnetic moments, as shown in Figure 10.

Discussion

In contrast to our previous work on the hydroxy-sulfates of copper(II) where only two crystal phases were identified in the whole range of reaction conditions (concentration, pH, and temperature), that of nickel(II) is more complex.[4] While several phases were identified by PXRD, DT-TGA, IR, and magnetization measurements from the powders obtained at low temperatures and at different concentration of reactants and pH, only one crystal phase was reproducibly prepared at high temperatures and in a wide range of concentration. This complex behavior with nickel is due to the high stability and low solubility of $Ni(OH)_2$ compared to $Cu(OH)_2$. The

situation with cobalt(II) and manganese(II) is even more complex due to the intermediate stability and solubility of $Co(OH)_2$ and $Mn(OH)_2$ and the stability of different coordination geometries (tetrahedral, pyramidal, and octahedral). The work on cobalt and manganese will be published shortly.

The structure determination evidences an original network consisting of chains of edge sharing Ni1 octahedra, Ni2 octahedral corners connected to the previous chains, and sulfate groups linking nickel octahedra first into layers and then into the 3D network. From DT-TGA results, we evidence that water molecules are strongly bonded to the network and, therefore, cannot be considered as water crystallization in agreement with the structure determination.

For IR spectroscopy, O−H vibrations appear as sharp bands and could be related to the absence of hydrogen bonds in the hydroxy-sulfate. This result agrees with the distances calculated from the neutron powder diffraction structure refinement (Table 2), showing that the shortest (H/D)···O contact is 1.935(10) Å (D1···O1). Even if some uncertainties exist concerning the precise location of H/D atoms, the absence of well-defined hydrogen bonds indicated by the sharp valence vibration bands of O−H bonds seems to be confirmed by neutron powder data. Concerning the sulfate groups, the bond lengths and angles slightly differ from ideal tetrahedral symmetry. However, such deviations are sufficient to reduce the local environment from T_d to C_{2v} for S1 and C_1 for S2. Therefore, in both cases S1 and S2, three bands are expected for ν_3 and ν_4 vibrations. As the bond lengths are very close to each other in both tetrahedra, IR spectroscopy does not distinguish S1 and S2. This is particularly evident for ν_4, as only three bands appear in the 650−600 cm^{-1} region. The three bands at higher wavenumbers (1109, 1159, and 1202 cm^{-1}) could be related to ν_3. While the band observed at 995 cm^{-1} is the ν_1 mode of SO_4, the 1035 cm^{-1} can be assigned to either ν_1 or ν_3.

Magnetic measurements show predominantly antiferromagnetic interactions in the paramagnetic region ($\theta < 0$ in the Curie−Weiss expression and continuous decrease of the χT product). A transition toward a 3D magnetic ordered state is revealed at around 30 K and confirmed by spontaneous magnetization and the λ-type anomaly in the specific heat. The increase of C_p at higher temperature is mainly due to the phonon contribution. The high temperature data have been fitted to the relationship $C_p = AT^{-2} + BT^3$, where the first term is ascribed to magnetic correlations while the second term deals with lattice contribution. After subtracting the latter, we get the specific heat of magnetic origin (□ in Figure 7).[25] It also allows the determination of the magnetic entropy, S_M; the experimental value of S_M associated with the magnetic transition (Figure 7) agrees with the theoretical one given by the following formula:[25]

$$S_M = R \ln(2S + 1) \text{ with } S = \text{spin value}$$

The presence of one peak in both components of the ac susceptibility versus temperature at 29 K leads us to conclude the presence of a net magnetization which is confirmed by the low field (5 Oe) dc magnetization measurements. The observation of a hysteresis loop at 2 K also confirms this observation. However, one has to note that the hysteresis loop is not characteristic of a ferromagnetic or even a ferrimagnetic sample since the magnetization does not reach saturation and the loop is restricted to a narrow applied field region. This behavior is better explained by a canted antiferromagnetic system. For the magnetic structure refinements in the Γ_2 irreducible representation, five free parameters could be refined, i.e., M_x, M_y, and M_z for Ni1, M_x and M_y for Ni2. Whereas M_y values are significant for both atoms, the values of M_x and M_z for Ni1 and of M_x for Ni2 are significantly smaller than their estimated standard deviations. Consequently, it results in a collinear antiferromagnetic structure without canting. However, the very small canting angle estimated from the net magnetization measured on the SQUID apparatus cannot indeed be resolved by the neutron powder diffraction technique.

Considering the magnetic structure, one observes a sequence $+ + - -$ along the Ni1 chain, as shown in Figure 9. Therefore, nearest neighbor Ni1 ions at short distances (Ni−Ni = 3.070 Å) are ferromagnetically coupled through OH1 and OH2 oxygen atoms whereas those at longer distances (Ni−Ni = 3.377 Å) are antiferromagnetically coupled through O2. Therefore, the Ni1 chains can be better described as AF chains where the moments of alternate dimers are antiparallel. If Ni2 octahedra are not directly connected to each other, coupling can take place either through sulfate groups or through Ni1 ions. In the latter case, each Ni2 is connected to four Ni1 ions by corner-sharing of two μ_3-hydoxo groups, OH1 and OH2. In the case of copper salts, it has been shown that the M−O−M angle has a strong influence on the nature of the magnetic interactions.[9,4] Coupling between nearest metallic cations is due to a superexchange via the oxygen atoms and is driven by the overlap between oxygen orbitals and metal orbitals, the sign of this interaction being directly related to the M−O−M angle. In our case, a similar observation can be made within the Ni1 chains: ferromagnetic interactions for angle values less than or equal to 97.6° and antiferromagnetic interactions for angle values greater than or equal to 102.75°. For Ni2 ions, AF coupling between Ni2 and its four neighbors is related to high angle values, 124.89° and 118.93° (Table 2). Finally, it can also be pointed out that if the magnetic moment of Ni1 ions, 2.00(4) μ_B, agrees with the expected value, it is not the case for Ni2 ions, 1.67(6) μ_B. This means that magnetic order is completely achieved at 1.4 K inside the Ni1 chains but not for Ni2. A possible explanation may concern the different coupling pathways. For Ni1 ions, coupling takes place through superexchange via the single oxygen atoms. In the case of Ni2, such ions are coupled by super-superexchange involving the sulfate groups via O−S−O bridges. One can therefore consider that the latter is much less effective even if a contribution by superexchange with the Ni1 ions can also be considered with Ni1−Ni2 distances of 3.550(12) and 3.608(13) Å, much longer than the intermetallic distances within the Ni1 chains.

(25) Carlin, R. L. *Magnetochemistry*; Springer-Verlag: Berlin/Heidelberg, 1986; p 165.

Conclusion

The controlled hydrothermal synthesis in the $NiSO_4-Ni(OH)_2$ system has provided good quality single crystals of $Ni_3(OH)_2(SO_4)_2(H_2O)_2$ and some other derivatives in powder form. Full nuclear and magnetic structures of the former have been resolved, and they confirm existing theoretical predictions of the dependence of the sign of the magnetic superexchange interactions on the angle of the Ni−O−Ni pathways. Accordingly, angles less than 98° favor ferromagnetic exchange, and those that are higher result in antiferromagnetic exchange. The coexistence of different exchange interactions results in a 3D antiferromagnetic ordering at 30 K and a weak spontaneous magnetization presumably due to a small canting of the magnetic sublattices. Further work on the other powdered phases is in progress.

Acknowledgment. This work was funded by the CNRS (France). We thank André Decian, Jean-Paul Lambour, and Alain Derory for technical assistance. D.S. thanks the ECC for financial support during his stay in Strasbourg.

Supporting Information Available: Crystallographic data in CIF format and additional figures. This material is available free of charge via the Internet at http://pubs.acs.org.

IC0345469